

Wouthuysen-Field Coupling in the 21 cm Region Around High Redshift Sources

Ishani Roy¹, Wen Xu², Jing-Mei Qiu³, Chi-Wang Shu¹, and Li-Zhi Fang²

ABSTRACT

The 21 cm emission and absorption from gaseous halos around the first generation of stars substantially depend on the Wouthuysen-Field (W-F) coupling, which relates the spin temperature with the kinetic temperature of hydrogen gas via the resonant scattering between Ly α photons and neutral hydrogen. Therefore, the existence of Ly α photons in the 21 cm region is essential. Although the center object generally is a strong source of Ly α photons, the transfer of Ly α photons in the 21 cm region is very inefficient, as the optical depth of Ly α photons is very large. Consequently, the Ly α photons ν_0 from the source may not be able to transfer to the entire 21 cm region timely to provide the W-F coupling. This problem is especially important considering that the lifetime of first stars generally is short. We investigate this problem with the numerical solution of the integrodifferential equation, which describes the kinetics of Ly α resonant photons in both physical and frequency spaces. We show that the photon transfer process in the physical space is actually coupled to that in the frequency space. First, the diffusion in the frequency space provides a shortcut for the diffusion in the physical space. It makes the mean time for the escape of resonant photon in optical depth τ media roughly proportional to the optical depth τ , not τ^2 . Second and more importantly, the resonant scattering is effective in bouncing photons with frequency $\nu \neq \nu_0$ back to ν_0 . This process can quickly restore ν_0 photons and establish the local Boltzmann distribution of the photon spectrum around ν_0 . Therefore, the mechanism of “escape via shortcut” plus “bounce back” enables the W-F coupling to be properly realized in the 21 cm region around first stars. This mechanism also works for photons injected into the 21 cm region by redshift.

Subject headings: cosmology: theory - intergalactic medium - radiation transfer - scattering

¹Division of Applied Mathematics, Brown University, Providence, RI 02912

²Department of Physics, University of Arizona, Tucson, AZ 85721

³Department of Mathematical and Computer Science, Colorado School of Mines, Golden, CO 80401

1. Introduction

The resonant scattering of Ly α photons with neutral hydrogen atoms leads to a local Boltzmann distribution of the photon spectrum around the Ly α frequency ν_0 with color temperature equal to the kinetic temperature T of hydrogen gas. Consequently, the spin temperature T_s of the hyperfine structure of neutral hydrogen will be coupled to the kinetic temperature of hydrogen gas. This is the so-called Wouthuysen-Field (W-F) coupling (Wouthuysen 1952; Field 1958, 1959). The W-F coupling is crucial to estimate the redshifted 21 cm signal from the halos of first generation of stars, because the deviation of the spin temperature from the temperature of cosmic microwave background (CMB) T_{cmb} is considered to be mainly caused by the W-F coupling (e.g. Furlanetto et al. 2006).

The lifetime of the first stars is short. The ionized and heated halos around the first luminous objects are strongly time-dependent. The time scale of the evolution of the expected 21 cm emission/absorption regions can be as small as 10^5 years (Cen 2006; Liu et al. 2007). Therefore, the 21 cm signal models based on the W-F coupling would be reasonable only if the time scale of the onset of the W-F coupling is less than that of the 21 cm region evolution. This time evolution has been studied very recently (Roy et al. 2009a, hereafter referred to as PaperI). It concludes that the local Boltzmann distribution can form within a time scale shorter than 10^5 years, but it would take 10^5 years or even longer to reach its saturation (time-independent) state. Therefore, it is legitimate to assume that the W-F coupling is taking place in the 21 cm emission/absorption regions, but the intensity of the photon flux is less than the time-independent solution.

PaperI studied, however, only the case of spatial homogeneity and isotropy. It is equivalent to assume that the Ly α photons are uniformly distributed in the entire 21 cm signal region. This assumption is not trivial. All the Ly α photons in the 21 cm regions come from first stars, either from direct emission of Ly α photons, or from the Hubble redshifted photons. On the other hand, the 21 cm regions are highly opaque for Ly α photons. The W-F coupling may not be uniformly available in the 21 cm signal region, if the time scale of the transfer of Ly α photons in the physical space is longer than that of the evolution of the 21 cm region.

The problem of Ly α photon transfer in optical thick media is not new. It has been addressed as early as 1960s in relation to the escape of resonant photons from opaque clouds (Osterbrock 1962; Harrington 1973; Avery & House 1968; Adams 1972). In these references it is shown that the diffusion of the photon distribution in the frequency space caused by the resonant scattering will be helpful to speed up the spatial diffusion. In the past decade, there are also many works on the escape of Ly α photons from high redshift objects with the mechanism of Hubble redshift (e.g. Miralda-Escude & Rees 1998; Loeb & Rybicki 1999;

Zheng & Miralda-Escude 2002; Haiman & Cen 2005; Tasitsiomi 2006; McQuinn et al. 2007). The Hubble redshifted Ly α photons are also easy to take spatial transfer. Although both the resonant scattering and the Hubble redshift are useful to solve the problem of Ly α photon transfer in the 21 cm region, they rely on the change of photon frequency from ν_0 to $\nu_0 \pm \Delta\nu$. Therefore, the local Boltzmann frequency distribution will be disturbed, even if it initially is in the state of local Boltzmann frequency distribution. Thus, it is unclear whether the W-F coupling keeps to work timely and uniformly in the 21 cm region.

In this context, a time-dependent solution of the kinetics of Ly α photons in both physical and frequency spaces of the 21 cm region is necessary. This is the topic of the current paper. We will show that the resonant scattering of Ly α photons is effective to solve the problem of spatial transfer in optical thick 21 cm region as well as to keep the W-F coupling working. On the other hand, for 21 cm regions of short lifetime objects, the cosmic expansion does not provide effective mechanism for the spatial transfer of Ly α photons.

Similar to PaperI, we use the numerical solution of the time-dependent integrodifferential equation of the radiative transfer with resonant scattering. The numerical solver is based on the weighted essentially non-oscillatory (WENO) scheme (Jiang & Shu 1996). WENO scheme is effective in solving Boltzmann equations (Carrillo et al. 2003, 2006) and radiative transfer (Qiu et al. 2006, 2007, 2008). The algorithm related to resonant scattering has also been given in Roy et al. (2009b). This numerical solver has successfully passed the tests of analytic solutions and conservation of photon number. Therefore, it is a good candidate for computing the current problem.

This paper is organized as follows. Section 2 addresses the physical problems of Ly α photon transfer in the 21 cm emission and absorption regions of luminous objects. Section 3 is on the time scale of the transfer of resonant scattering in the frequency space. Section 4 presents Ly α photon transfer in the frequency and physical spaces. These results can be used for the 21 cm signal region (§5). Discussion and conclusion are given in Section 6. The details of the numerical implementation are given in the Appendix.

2. Radiative transfer problem of the 21 cm region

2.1. Basic properties of the 21 cm region

The property of the ionized and heated regions around an individual luminous object is dependent on the luminosity (or mass), the spectrum of UV photon emission, and the time-evolution of the center object (Cen 2006; Liu et al. 2007). We will not work on a specific model, but consider only the common features. These halos generally consist of

three spheres. The most inner region of the halo is the highly ionized Strömgen sphere, or the HII region, in which the fraction of neutral hydrogen $f_{\text{HI}} = n_{\text{HI}}/n_{\text{H}}$ is no more than 10^{-5} , where n_{HI} and n_{H} are, respectively, the number densities of neutral hydrogen HI and total hydrogen. The temperature of the HII region is about 10^4 K. The physical radius of this sphere is in the range of a few to a few tens of kpc. The second region is the 21 cm emission shell, which is just outside the HII region. The physical size of this shell is similar to that of the HII sphere. The temperature of hydrogen gas in the emission shell is in the range $10^2 < T < 10^4$ K due to the heating of UV photons. The fraction f_{HI} is in the range of 0.1 to 1. The third region is the 21 cm absorption shell, which is outside the 21 cm emission region. The physical size is on the order of 100 kpc. The temperature of this region is lower than $T_{\text{cmb}} = T_{\text{CMB}}(1+z)$, where T_{CMB} is the temperature of CMB today. The time scale of the formation of the halos is about 10^6 years. The lifetime of the halos is about the same as the lifetime of the first stars.

At the epoch of redshift $z \simeq 20$, the reionization region consists of isolated patches around first sources. Most Ly α photons in the 21 cm regions should come from the central source and the subsequent re-emission processes. If one can estimate the center object as a Ly α emitter, the emission of Ly α photons in number per unit time would be about $dN_{\text{Ly}\alpha}/dt = 10^{53} \text{ s}^{-1}$. The recombination of HII and electron in the Strömgen sphere is also a source of Ly α photons. If the physical radius of the Strömgen sphere is ~ 10 kpc, the emission intensity is about $dN_{\text{Ly}\alpha}/dt = 10^{49} \text{ s}^{-1}$.

Using the parameters of the concordance Λ CDM model, the optical depths of photons with Ly α resonant frequency ν_0 in the 21 cm region are

$$\tau(\nu_0) = n_{\text{HI}}\sigma_0 R = 4.9 \times 10^6 f_{\text{HI}} \left(\frac{T}{10^4}\right)^{-1/2} \left(\frac{1+z}{20}\right)^3 \left(\frac{\Omega_b h^2}{0.022}\right) \left(\frac{R}{10\text{kpc}}\right), \quad (1)$$

where σ_0 is the cross section of the resonant scattering at the frequency ν_0 , R is the physical size of the considered sphere, and τ is the distance R in the units of the mean free path of ν_0 photons at redshift z . Eq.(1) shows that the optical depth of the 21 cm signal regions with $f_{\text{HI}} \geq 0.1$ is $\tau(\nu_0) \geq 10^6$.

It is also useful to define a dimensionless time $\eta = cn_{\text{HI}}\sigma_0 t$ as

$$t = \eta/cn_{\text{HI}}\sigma_0 = 6.7 \times 10^{-3} f_{\text{HI}}^{-1} \left(\frac{T}{10^4}\right)^{1/2} \left(\frac{20}{1+z}\right)^3 \left(\frac{0.022}{\Omega_b h^2}\right) \eta \text{ yrs}. \quad (2)$$

This is the time in the units of mean free flight-time. For a time scale $t \simeq 10^5$ yrs, the scale of η is $\simeq 10^7$.

2.2. Problems with the W-F coupling

There are, at least, two radiative transfer problems with the W-F coupling in the 21 cm regions: A.) How to provide enough Ly α photons in such opaque medium? B.) Can the radiative transfer in the 21 cm region keep the W-F coupling to work well?

If photons *always* keep the frequency ν_0 , their spatial diffusion can be described as a random walk process (Chandrasekar 1943). The mean number of scattering required for the diffusion over a range R is on the order of τ^2 . Thus, the time for the diffusion over the 21 cm range is $\eta \simeq \tau^2$, corresponding to the time $t = \tau^2/cn_{\text{HI}}\sigma_0 \geq 10^{12}$ years. This diffusion mechanism, obviously, is useless for the 21 cm regions.

The time scale of the diffusion would be substantially reduced if the frequency of the Ly α photons can have a small shift from ν_0 to $\nu = \nu_0 \pm \Delta\nu$, because the optical depth τ at the frequency $\nu_0 \pm \Delta\nu$ is significantly less than $\tau(\nu_0)$. One can estimate the frequency shift $\Delta\nu$ by the condition of optical depth $\tau(\nu_0 \pm \Delta\nu) \simeq 1$, which is

$$\tau(\nu_0) \frac{\phi(x, a)}{\phi(0, a)} \leq 1 \quad (3)$$

where $\phi(x, a)$ is the Voigt function for the resonant line ν_0 profile as (Hummer 1965)

$$\phi(x, a) = \frac{a}{\pi^{3/2}} \int_{-\infty}^{\infty} dy \frac{e^{-y^2}}{(x-y)^2 + a^2} \quad (4)$$

where the dimensionless variable x is defined by $x = (\nu - \nu_0)/\Delta\nu_D$ and $\Delta\nu_D = \nu_0 v_T/c$ is the Doppler broadening of hydrogen gas with thermal velocity $v_T = \sqrt{k_b T/2m_{\text{H}}}$. Therefore, x measures the frequency deviation $\Delta\nu = |\nu - \nu_0|$ in the units of the Doppler broadening. The parameter a in eq.(4) is the ratio of the natural to the Doppler broadening. For Ly α line, $a = 2.35 \times 10^{-4}(T/10^4)^{-1/2}$. In terms of x , the solution of eq.(3) is $x \geq 3$.

An effective mechanism of the frequency shift is given by the diffusion of the photon distribution in the frequency space. Considering this mechanism, the number of scattering required for diffusion over a physical distance R is no longer equal to τ^2 , but roughly on the order of τ (Osterbrock 1962; Harrington 1973; Avery & House 1968; Adams 1972). Since $\tau \propto R$, the time scale of the spatial diffusion over size R is comparable to R/c . Problem A would then be solved.

Problem B still remains. If photons with the frequency $\nu < \nu_0 - \Delta\nu$ or $\nu > \nu_0 + \Delta\nu$ take a faster spatial diffusion than the ν_0 photons, how can we keep the W-F coupling to work? Without ν_0 photons, one cannot have a local Boltzmann distribution around ν_0 . Therefore, the photons with the frequency $\nu < \nu_0 - \Delta\nu$ or $\nu > \nu_0 + \Delta\nu$ should be brought back to the

frequency ν_0 . We must study whether the frequency space diffusion mechanism can restore ν_0 photons from photons with the frequency $\nu \neq \nu_0$.

Cosmic expansion also leads to a deviation of photon frequency from ν_0 to a lower one $\nu_0 - \Delta\nu$, which speeds up the spatial transfer. However, we also need a mechanism to restore Ly α photons from Hubble redshifted photons. Therefore, in terms of the W-F coupling in the 21 cm region, we must study the kinetics of Ly α photons in both physical and frequency spaces.

3. Radiative transfer of resonant photons in the frequency space

3.1. Equations

We first estimate the time scale needed for the frequency shift. We can use the radiative transfer equation of a homogeneous and isotropically expanding infinite medium consisting of neutral hydrogen. The equation of the mean intensity J in terms of the photon number is (Hummer & Rybicki 1992; Rybick & Dell’antonio 1994)

$$\begin{aligned} \frac{\partial J(x, \eta)}{\partial \eta} &= -\phi(x, a)J(x, \eta) \\ &+ \int \mathcal{R}(x, x'; a)J(x', \eta)dx' + \gamma \frac{\partial J}{\partial x} + S(x, \eta). \end{aligned} \quad (5)$$

The parameter γ^{-1} measures the number of scattering during a Hubble time, given by

$$\gamma^{-1} = 1.4 \times 10^6 h^{-1} f_{\text{HI}} \left(\frac{0.25}{\Omega_M} \right)^{1/2} \left(\frac{\Omega_b h^2}{0.022} \right) \left(\frac{1+z}{20} \right)^{3/2}. \quad (6)$$

The re-distribution function $\mathcal{R}(x, x')$ gives the probability of a photon absorbed at the frequency x' , and re-emitted at the frequency x . It depends on the details of the scattering (Henyey 1941; Hummer 1962; Hummer, 1969). If we consider coherent scattering without recoil, the re-distribution function with the Voigt profile eq.(4) is

$$\begin{aligned} \mathcal{R}(x, x'; a) &= \\ \frac{1}{\pi^{3/2}} \int_{|x-x'|/2}^{\infty} e^{-u^2} \left[\tan^{-1} \left(\frac{x_{\min} + u}{a} \right) - \tan^{-1} \left(\frac{x_{\max} - u}{a} \right) \right] du \end{aligned} \quad (7)$$

where $x_{\min} = \min(x, x')$ and $x_{\max} = \max(x, x')$. In the case of $a = 0$, i.e. considering only the Doppler broadening, the re-distribution function is

$$\mathcal{R}(x, x') = \frac{1}{2} e^{2bx' + b^2} \text{erfc}[\max(|x + b|, |x' + b|)], \quad (8)$$

where the parameter $b = h\nu_0/mv_Tc = 2.5 \times 10^{-4}(10^4/T)^{1/2}$ is due to the recoil of atoms. The re-distribution function of eq.(8) is normalized as $\int_{-\infty}^{\infty} \mathcal{R}(x, x')dx' = \phi(x, 0) \equiv \phi_g(x) = \frac{1}{\sqrt{\pi}}e^{-x^2}$. The numerical algorithm to solve eq.(5) has been given in Roy et al. (2009a, 2009b).

3.2. Time scales of the frequency shift

On the right hand side of eq. (5), the first term is the absorption at the resonant frequency x , the second term is the re-emission of photons with frequency x by scattering, and the third term describes the Hubble redshift of photons. We first solve eq. (5) by dropping the terms of absorption and re-emission. The equation is

$$\frac{\partial J}{\partial \eta} = \gamma \frac{\partial J}{\partial x} + S(x, \eta). \quad (9)$$

Assuming the source is $S = C\phi_s(x)$, where $\phi_s(x)$ is the normalized frequency profile of the source photons. The analytic solution of eq.(9) is (Rybicki & Dell’antonio, 1994)

$$J(x, \eta) = J(x + \gamma\eta, 0) + C\gamma^{-1} \int_x^{x+\gamma\eta} \phi_s(x')dx' \quad (10)$$

where $J(x, 0)$ is the initial flux. Define the mean frequency by

$$\bar{x}(\eta) \equiv \frac{\int xJ(\eta, x)dx}{\int J(\eta, x)dx}. \quad (11)$$

If the initial flux is $J(x, 0) = 0$, one can show that for any profile $\phi_s(x)$ we have

$$\bar{x}(\eta) = -\gamma\eta/2. \quad (12)$$

As expected, the speed of redshift $d\bar{x}/d\eta$ is a constant. For the Hubble expansion, a frequency shift x needs a time $\eta \simeq \gamma^{-1}x$. Thus, in order to have the frequency shift $x \geq 3$, the time scale is $\eta \geq 6 \times 10^6$, corresponding to $t \geq 4 \times 10^4$ years. This scale seems to be short enough compared with the lifetime of first stars. However, Hubble redshift is less effective comparing with the resonant scattering. This point can be seen in Figure 1, which gives the solution of eq.(5) with the re-distribution function eq.(8). The source is taken to be $S(x) = \phi_g(x) = (1/\sqrt{\pi})e^{-x^2}$. We also take the parameter γ to be 10^{-6} [eq.(6)], and ignore recoil, i.e. $b = 0$.

Figure 1 shows that the diffusion in the frequency space leads to a flat plateau with width $|x| \leq 3$ when η is as small as $\eta \simeq 10^4$, or $t \simeq 10^2$ years. This time scale is much less than that of the Hubble redshift. Therefore, the major mechanism to produce photons with frequency $|x| \geq 3$ is given by the resonant scattering.

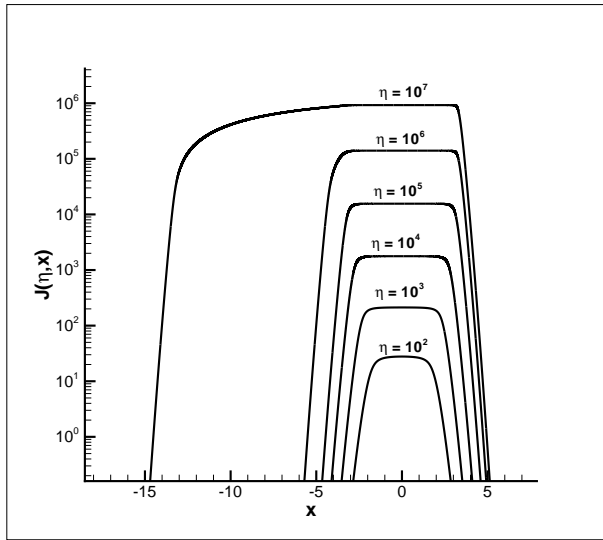


Fig. 1.— Solutions $J(\eta, x)$ of eq. (5) with the re-distribution function eq.(8). Parameters $b = 0$, and $\gamma = 10^{-6}$.

3.3. Bounce back mechanism

From Figure 1, we can see that the profile of photons are almost symmetric with respect to $x = 0$ (or to $\nu = \nu_0$) until about the time $\eta = 10^6$. The redshift effect can only be seen from the curve of $\eta \geq 10^6$. That is, the resonant scattering impedes cosmic redshift. The impediment is due to the “bounce back” of resonant scattering. Regardless of whether the frequency of the absorbed photons is larger or smaller than ν_0 , the mean frequency of the re-emitted photons is always ν_0 . Therefore, the resonant scattering will bring back some redshifted photons to the frequency ν_0 . Thus the net effect of resonant scattering (absorption and re-emission) is, on average, to bounce redshifted photons back to the resonant frequency ν_0 , and to restore the symmetry with respect to $x = 0$. This bounce back mechanism is the key of restoring ν_0 photons and the W-F coupling (see §4).

To illuminate the bounce back effect, we calculate the mean frequency $\bar{x}(\eta)$ for the solutions shown in Figure 1. The result is plotted in Figure 2. The solution of pure cosmic redshift eq.(12) is also shown in Figure 2 as the dashed curve. We can see from Figure 2 that the speed of photon frequency shift $d\bar{x}/d\eta$ when considering resonant scattering is in general less than that in the case of pure cosmic redshift. When the time η is large, many photons have been redshifted out of the frequency range of $\phi_g(x)$. In this case, the “bounce back” effect ceases, and redshift speed is recovered to $d\bar{x}/d\eta = -\gamma/2$. From Figure 2 one can see once again that the Hubble redshift can produce frequency shift from $x = 0$ to $|x| \simeq 3$ only when $\eta \geq 10^7$, or $t \simeq 10^5$ years. This time scale may not be short enough to match the

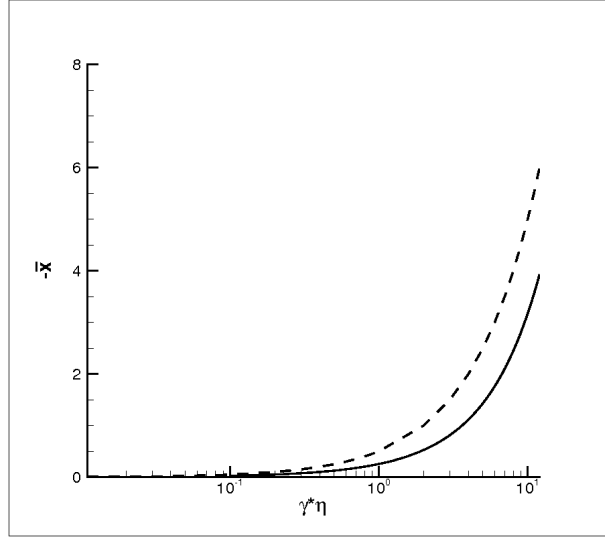


Fig. 2.— \bar{x} vs. $\gamma\eta$ for the solution shown in Figure 1 (solid) and the solution of eq.(12) (dashed).

21 cm region with a short lifetime. When the time scale of resonant scattering is less than the time scale of Hubble expansion, the frequency shift of the Hubble expansion slows down significantly by the resonant scattering.

4. Radiative transfer (RT) of Ly α photons in the 21 cm regions

4.1. RT equation in spherical halo

Considering a photon source located at the central region of a uniformly distributed expanding medium, we can use the RT equation of the specific intensity $I(\eta, r, x, \mu)$ as follows

$$\begin{aligned} \frac{\partial I}{\partial \eta} + \mu \frac{\partial I}{\partial r} + \frac{(1 - \mu^2)}{r} \frac{\partial I}{\partial \mu} - \gamma \frac{\partial I}{\partial x} = \\ -\phi(x)I + \int \mathcal{R}(x, x')I(\eta, r, x', \mu')dx'd\mu' + S, \end{aligned} \quad (13)$$

where $\mu = \cos \theta$ is the direction relative to the radius vector \mathbf{r} . The dimensionless coordinate r is rescaled from the physical coordinate r_p as

$$r_p = 2.1 \times 10^{-3} f_{\text{HI}}^{-1} \left(\frac{T}{10^4} \right)^{1/2} \left(\frac{20}{1+z} \right)^3 \left(\frac{0.022}{\Omega_b h^2} \right) r \text{ pc}. \quad (14)$$

With these variables, the propagation of a signal with the speed of light will be described by the equation $r = \eta + \text{const}$. It would still be reasonable to use the isotropic approximation of the re-distribution (Mihalas et al. 1976).

When the optical depth is large, the Eddington approximation would be proper. It is

$$I(\eta, r, x, \mu) \simeq J(\eta, r, x) + 3\mu F(\eta, r, x) \quad (15)$$

where $J(\eta, r, x) = \frac{1}{2} \int_{-1}^{+1} I(\eta, r, x, \mu) d\mu$ is the angularly averaged specific intensity and $F(\eta, r, x) = \frac{1}{2} \int_{-1}^{+1} \mu I(\eta, r, x, \mu) d\mu$ is the flux. Defining $j = r^2 J$ and $f = r^2 F$, Eq.(13) yields the equations of j and f as

$$\frac{\partial j}{\partial \eta} + \frac{\partial f}{\partial r} = -\phi(x)j + \int \mathcal{R}(x, x') j dx' + \gamma \frac{\partial j}{\partial x} + r^2 S, \quad (16)$$

$$\frac{\partial f}{\partial \eta} + \frac{1}{3} \frac{\partial j}{\partial r} - \frac{2}{3} \frac{j}{r} = -\phi(x)f. \quad (17)$$

The numerical algorithm for eqs.(16) and (17) is given in the Appendix.

Since photons with frequency shifted away from ν_0 would be optical thin, the equations (16) and (17) will no longer be a good approximation when the frequency of photons is shifted to the optical thin case. From Figures 1 and 2, one can see that within $\eta \leq 10^6$, most photons are still trapped in the frequency $|x| \leq 3$, for which the optical depth is larger than 1. Therefore, the Eddington approximation would be proper, at least, until η is as large as about 10^6 .

4.2. Diffusion in the physical space

We first solve the equations (16) and (17) by dropping all terms on the transfer in frequency. It has been shown that the source term can be replaced by a boundary condition of f and j at $r = r_0$ (Qiu et al. 2006). The equations then become

$$\frac{\partial j}{\partial \eta} + \frac{\partial f}{\partial r} = 0, \quad (18)$$

$$\frac{\partial f}{\partial \eta} + \frac{1}{3} \frac{\partial j}{\partial r} - \frac{2}{3} \frac{j}{r} = -f. \quad (19)$$

We take the boundary condition at $r_0 = 1$ to be

$$j(\eta, 1) = 3S_0, \quad f(\eta, 1) = S_0 = 10^6. \quad (20)$$

Since eqs.(18) and (19) are linear, the parameter S_0 is not important if we are only interested in the shape of j and f as function of η and r . The initial condition is taken to be

$$j(0, r) = f(0, r) = 0. \quad (21)$$

The solution of $f(\eta, r)$ is presented in Figure 3. The dashed line is $f = S_0 = 10^6$, which is the time-independently exact solution of eq.(18). It is a horizontal straight line because the flux $f = r^2 F$ is r -independent and satisfies the conservation of the photon number. Figure 3 shows that the spatial size r of $f(\eta, r)$ roughly satisfies $r \propto \sqrt{\eta}$. Therefore, without resonant scattering, the diffusion basically is a random walk process as discussed in §2.2.

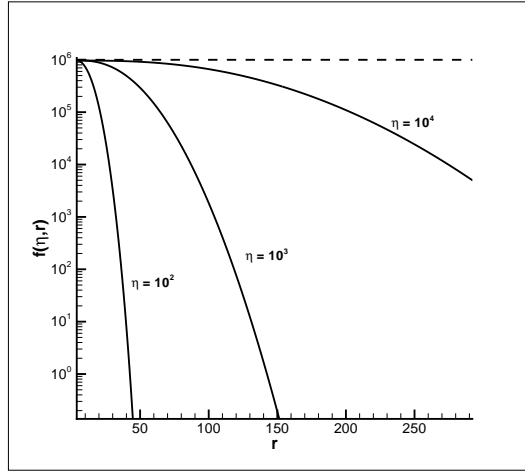


Fig. 3.— The solution $f(\eta, r)$ of eqs.(18) and (19). The straightline is $f = S_0 = 10^6$.

We now turn to the solution of eqs.(16) and (17) with resonant scattering and Hubble redshift. The relevant parameters are given by $b = 0$ and $\gamma = 10^{-5}$. We use the boundary condition at $r = 0$

$$j(\eta, 0, x) = 0, \quad f(\eta, 0, x) = S_0 \phi_s(x) \quad (22)$$

where the frequency profile is taken to be the Gaussian profile, i.e. $\phi_s(x) = \phi_g(x)$. The parameter S_0 is still taken to be 10^6 . The initial condition is similar to eq.(21), i.e. $j(0, r, x) = f(0, r, x) = 0$. The solutions of $f(\eta, r, x)$ are plotted in Figure 4.

All the solutions of Figure 4 show two remarkable peaks at $x \simeq \pm(2 - 3)$ for all radius r . The amplitude of $f(\eta, r, x)$ at the peaks is higher than that at $x = 0$ by a factor of 10 to 10^2 . It shows that the flux is dominated by photons with frequency $x \simeq \pm(2 - 3)$. That is, the spatial transfer is carried out by photons of $x \simeq \pm(2 - 3)$. The amplitude of the flux at the saturated peaks is basically r -independent, and the saturated values of $\int f(\eta, r, x) dx$ are r -independent. This is consistent with the conservation of the photon number.

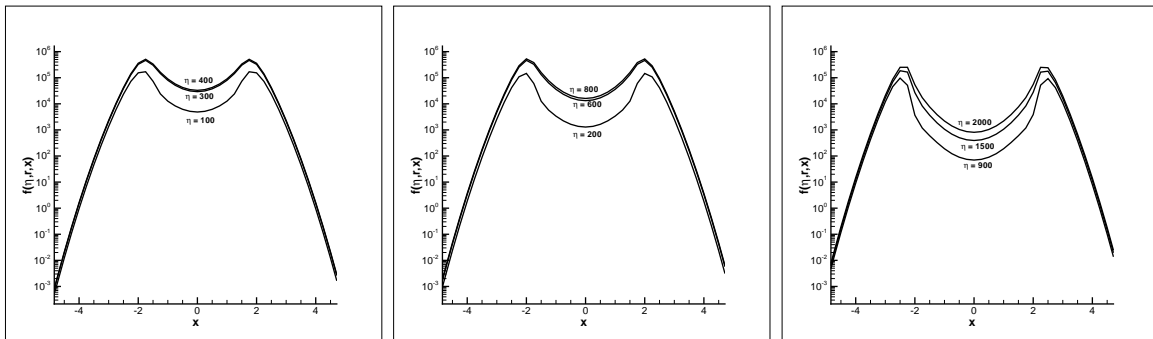


Fig. 4.— The flux $f(\eta, r, x)$ of the solutions of eqs.(16) and (17) at $r = 50$ (left), 100 (middle) and 500 (right). The frequency profile of the source is $\phi_g(x) = (1/\sqrt{\pi})e^{-x^2}$.

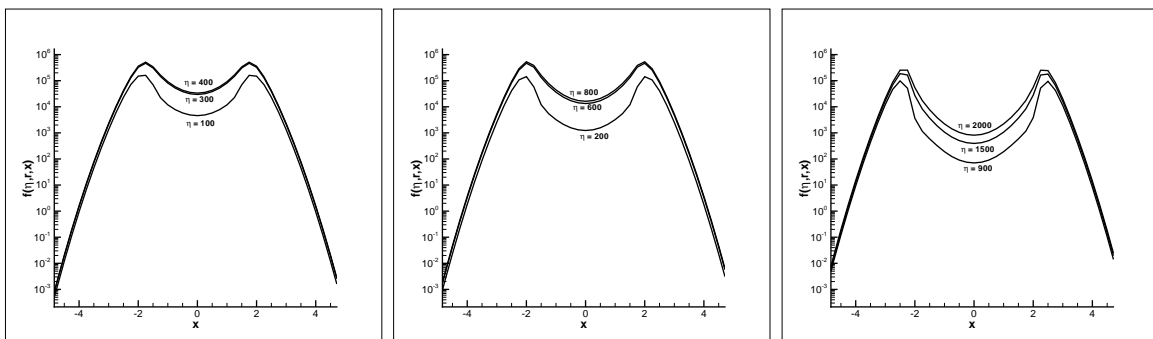


Fig. 5.— The flux $f(\eta, r, x)$ of the solutions of eqs.(16) and (17) at $r = 50$ (left), 100 (middle) and 500 (right). The frequency profile of the source is $\phi_s(x) = (1/\sqrt{\pi/2})e^{-2x^2}$.

More importantly, the amplitude of the peaks approaches its saturation at about $\eta \simeq 200$ for $r = 50$, $\eta \simeq 400$ for $r = 100$, and $\eta \simeq 2,000$ for $r = 500$. That is, the time η needed for the spatial transfer over size r is roughly proportional to r . This is very different from the random walk relation $\eta \propto r^2$, or the results shown in Figure 3.

It should be emphasized that the photons at the two peaks are not only those with $x \simeq \pm(2-3)$ directly from the source $S_0\phi_s(x)$, but also include the photons with frequency-shift from $x \simeq 0$ to $x \simeq \pm(2-3)$. This point can be shown by a source of the profile with smaller width, say, $\phi_s(x) = (1/\sqrt{\pi/2})e^{-2x^2}$. In Figure 5, we plot the results. For the source of $\phi_s(x) = (1/\sqrt{\pi/2})e^{-2x^2}$, the number of photons with $x \simeq \pm(2-3)$ is much less than that of the source $(1/\sqrt{\pi})e^{-x^2}$. We can see that all the features in Figure 5 are the same as those in Figure 4. The two peaks are still located at $x \simeq \pm(2-3)$. The time scale for approaching saturation in Figure 5 is also the same as that in Figure 4.

Therefore, photons at the peaks of $x \simeq \pm(2-3)$ should come from the frequency-shift

from $x = 0$ to $x \simeq \pm(2 - 3)$ by resonant scattering. That is, resonant scattering provides a shortcut of the spatial transfer: first to shift $x = 0$ photons to $x \simeq \pm(2 - 3)$ photons, and then to speed up spatial transfer. This mechanism is the same as that for the escape of resonant photons from opaque clouds (Osterbrock 1962; Harrington 1973; Avery & House 1968; Adams 1972). It allows the Ly α photons to be able to transfer over to the 21 cm regions in time η proportional to its size r .

4.3. Resonant photon restoration and W-F coupling onset

We have mentioned in §4.2 that the flux $f(\eta, r, x)$ is lacking ν_0 (or $x = 0$) photons even when f approaches its saturation. This is, obviously, not good for the W-F coupling. However, we found that the situation may not be so if we consider the solution of the mean specific intensity j . Figure 6 presents the solution $j(\eta, r, x)$ of equations (16) and (17) at $r = 50, 100$ and 500 . The parameters $b = 0$ and $\gamma = 10^{-5}$ are the same as the solutions in Figure 4. The results are given in Figure 6.

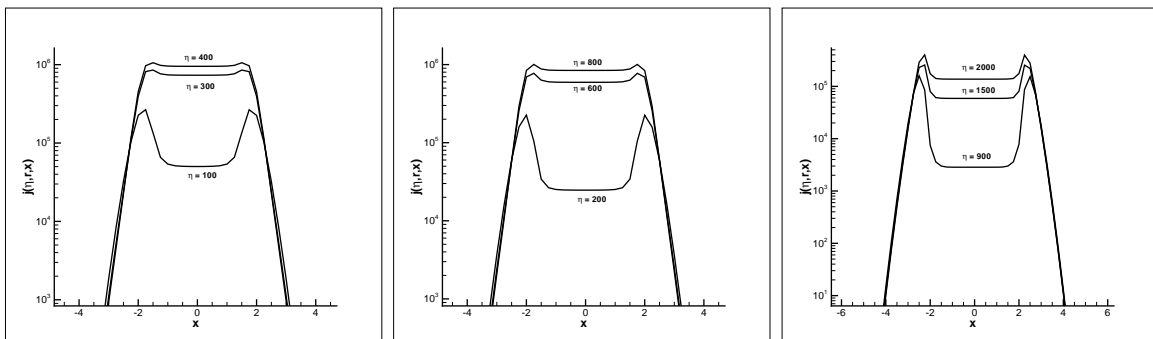


Fig. 6.— The mean intensity $j(\eta, r, x)$ of eqs.(16) and (17) at $r = 50$ (left), 100 (middle) and 500 (right).

When the time η is small, $j(\eta, r, x)$ is similar to $f(\eta, r, x)$, having a valley around $x = 0$ and two peaks at $x \simeq \pm(2 - 3)$. However, different from the flux $f(\eta, r, x)$, the amplitude of $j(\eta, r, x)$ around $x = 0$ is quickly increasing. In the saturated state it is about the same as the peaks. That is, although the flux always has a valley around $x = 0$, the ν_0 photons are quickly restored in the mean intensity. The time scale of approaching its saturated state is also proportional to r , not r^2 . Therefore, the restoration of resonant photons is due to the resonant scattering “bounce back” (§3.3), which pushes photons with frequency $x \simeq \pm(2 - 3)$ back to $x \simeq 0$.

The shape of $j(\eta, r, x)$ around $x = 0$ is a flat plateau, which is similar to that in Figure

1. As have been shown in PaperI, the flat plateau of $j(\eta, r, x)$ at $b = 0$ will become the local Boltzmann distribution if the recoil is considered. We can expect that the flat plateau of Figure 6 will also show a local Boltzmann distribution if $b \neq 0$. We calculate the solutions $j(\eta, r, x)$ and $f(\eta, r, x)$ of eqs. (16) and (17) at $r = 500$ with the same parameters as those in Figure 6, but with $b = 0.3$. We use a large b , because it is easier to see the slope of the local Boltzmann distribution. The results are given in Figure 7.

Figure 7 clearly shows a local Boltzmann distribution within the range $|x| \leq 2$ as

$$j(\eta, r, x) \simeq j(\eta, r, 0)e^{-2bx} = j(\eta, r, 0)e^{-h(\nu-\nu_0)/k_B T}. \quad (23)$$

We find the slope to be $\ln j(\eta, 0) - \ln j(\eta, 1) = 0.59$, which is well consistent with $2b = 0.6$. Figure 7 shows that at $r = 500$, the onset of the W-F coupling can occur as early as $\eta = 900$, but the amplitude of the local Boltzmann distribution at that time is much lower than its saturated value by a factor of 10^2 . The amplitude of the local Boltzmann distribution is substantially increasing with time. Therefore, the “bounce back” mechanism keeps the W-F coupling to work with a timescale η larger than a few hundreds, i.e. a few hundred collisions. This result is the same as that in PaperI.

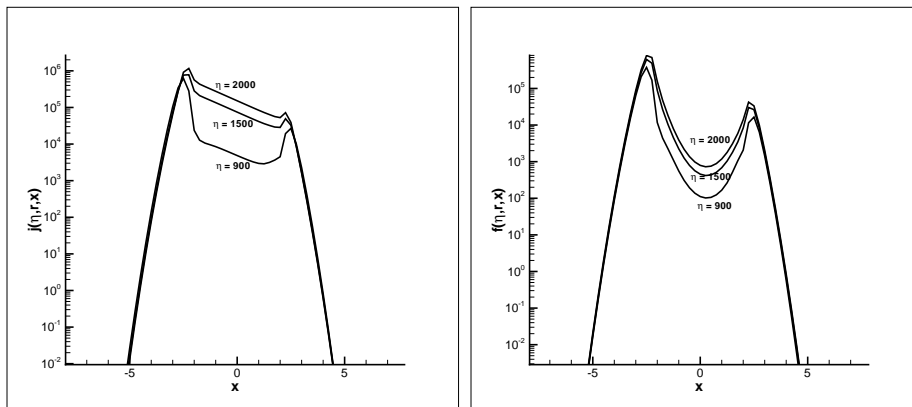


Fig. 7.— The mean intensity $j(\eta, r, x)$ (left) and flux $f(\eta, r, x)$ (right) of the solution of eqs.(16) and (17) at $r = 500$. The recoil parameter is taken to be $b = 0.3$.

The solution of the flux $f(\eta, r, x)$ in Figure 7 is not very different from that in Figure 4. The only difference between the two figures is that the former is asymmetric with respect to $x = 0$, i.e. the peak at $x < 0$ is stronger than that of $x > 0$, while the latter is symmetric. This is simply due to the recoil of $b \neq 0$ leading more photons to move to $x < 0$. Neither flat plateau nor local Boltzmann distribution is shown in the flux $f(\eta, r, x)$. There is always a valley around ν_0 even when $f(\eta, r, x)$ is in its saturated state. It once again indicates that the flux is dominated by photons of $x \simeq \pm(2 - 3)$.

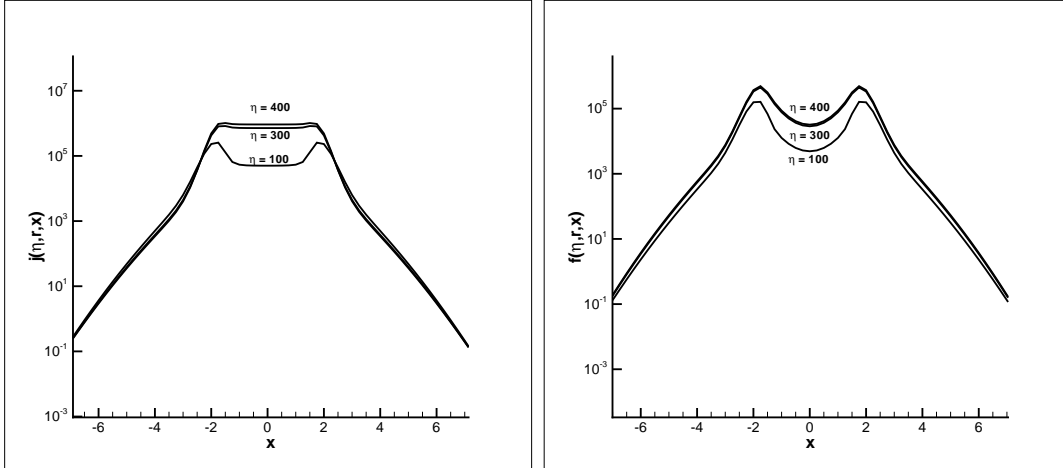


Fig. 8.— The mean intensity $j(\eta, r, x)$ (left) and flux $f(\eta, r, x)$ (right) of the solution of eqs.(16) and (17) with the Voigt profile eq.(4) and re-distribution function eq.(7). The parameters are taken to be $r = 50$ and $a = 10^{-2}$.

The two components f and j of the Eddington approximation are effective in revealing the functions of the resonant scattering. The flux $f(\eta, r, x)$ describes the photons in transit. It shows that the spatial transfer within opaque media is mainly via photons with frequency shifted to $x \simeq \pm(2 - 3)$, which are easy for escaping. The mean intensity $j(\eta, r, x)$ describes the restoration of $x = 0$ photons and the onset of the W-F coupling. Therefore, $f(\eta, r, x)$ shows a deep valley around $x = 0$ (or ν_0), while $j(\eta, r, x)$ shows a plateau.

In Figure 8, we present the the solutions of mean intensity $j(\eta, r, x)$ and flux $f(\eta, r, x)$ given by eqs.(16) and (17) with the Voigt profile eq.(4) and re-distribution function eq.(7). As expected, Figure 8 has the Lorentz wings. However, in the center part $|x| \leq 3$, Figure 8 shows the same features as Figures 4 and 6. That is, the mechanism of “escape via shortcut” plus “bounce back”, which mainly relies on photons with $|x| < 3$, still works well. The Lorentz wing only leads to long tails in the profiles of j and f in the range $|x| > 3$, and the wings have very low amplitudes.

4.4. Effect of injected photons

Hubble redshift is another mechanism to produce photons with frequency $\sim \nu_0$, which also have the problems of the spatial transfer and the W-F coupling. Since the 21 cm region basically is optical thin for photons with $x > 3$, we first model the cosmic redshift by a photon source with the profile $\phi_s(x) = \phi_g(x - 3)$. The solutions of $f(\eta, r, x)$ and $j(\eta, r, x)$

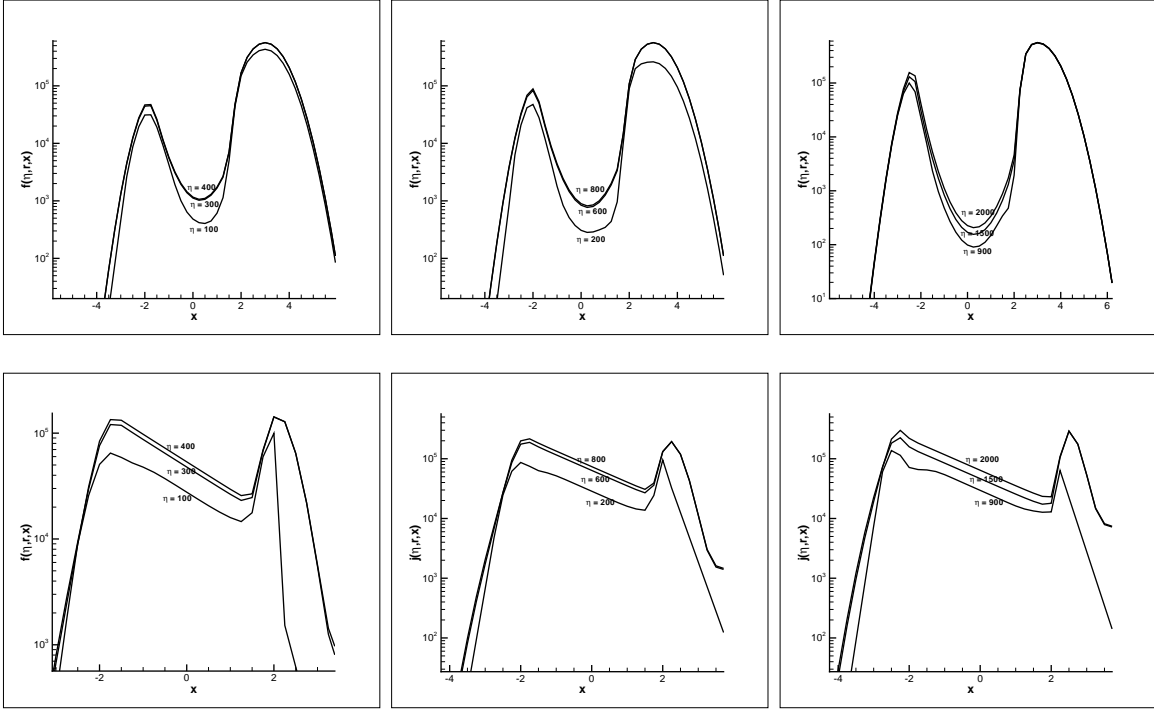


Fig. 9.— The mean intensity $j(\eta, r, x)$ and flux $f(\eta, r, x)$ of eqs.(16) and (17) at $r = 50$ (left), 100 (middle) and 500 (right). parameter $b = 0.3$. The frequency profile of the source is $\phi_s(x) = \phi_g(x - 3)$.

with the same parameters as in Figure 7 are shown in Figure 9.

Although the injected photon has a peak at $x = 3$, the flux $f(\eta, r, x)$ in Figure 9 still shows two peaks at $x \simeq \pm(2-3)$. The peak at $x \simeq (2-3)$ is higher than that at $-x \simeq (2-3)$. It is simply because the photon source is at $x = 3$. The peak at $x < 0$ is also much higher than $f(\eta, r, x)$ at $x = 0$. That is, even though the source photon is at $x = 3$, the spatial transfer is still dominated by photons of both $x \simeq (2 - 3)$ and $x \simeq -(2 - 3)$. The mean intensity $j(\eta, r, x)$ shows once again a perfect local Boltzmann distribution with slope $2b$ in the range $-2 < x < 2$ (eq.(23)). Any photons injected by the redshift into the 21 cm region will quickly join the W-F coupling by the bounce back mechanism.

We now model the source with a continuous frequency spectrum: $\phi_s(x) = S_0$ within $|x| \leq 10$, and $\phi_s(x) = 0$ at $|x| > 10$. The solutions of the mean intensity $j(\eta, r, x)$ and flux $f(\eta, r, x)$ of eqs.(16) and (17) are shown in Figure 10, in which the other parameters are the same as those in Figure 8. We can see that in the center part $|x| \leq 3$, $j(\eta, r, x)$ and $f(\eta, r, x)$ have the same features as in Figure 8. This result is expected, as the center

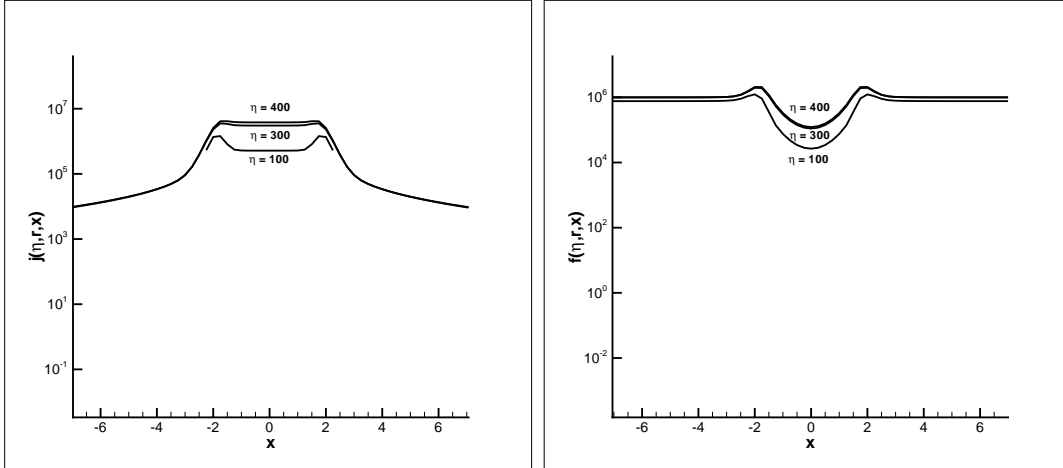


Fig. 10.— The mean intensity $j(\eta, r, x)$ and flux $f(\eta, r, x)$ of eqs.(16) and (17) with the Voigt profile eq.(4) and re-distribution function eq.(7). The frequency profile of the source is flat, i.e. $\phi_s(x)$ is equal to S_0 within $|x| \leq 10$, and to zero at $|x| > 10$.

part has contributions from the photons redshifted to $|x| \leq 3$ from $x > 3$. Figure 9 shows that the source of $\phi_g(x - 3)$ does not change the mechanism of “escape via shortcut” plus “bounce back”, and therefore, the source with a continuous frequency spectrum will keep these features as well.

4.5. Effect of the Hubble redshift

Although the cosmic expansion is considered in all the above-mentioned solutions, the effect of cosmic expansion seems to be negligible. It is because the optical depth is large and the parameter γ is very small. The number of resonant scattering within the Hubble time is very large. The cosmic expansion is too small in one free flight time. The “bounce back” is dominant.

When f_{HI} is smaller, optical depth of the ν_0 photons is smaller, and γ is larger, the effect of the Hubble redshift would appear. Figure 11 presents the solution $f(\eta, r, x)$ and $j(\eta, r, x)$ of eqs.(16) and (17) with the same parameters as those in Figures 4 and 6, except that the parameter $\gamma = 10^{-3}$ is large. Both $j(\eta, r, x)$ and $f(\eta, r, x)$ show the same features as in Figures 4 and 6. The Hubble redshift makes the profile to be asymmetric with respect to $x = 0$. The red wing is stronger than the blue wing. $j(\eta, r, x)$ still shows a flat plateau in the range $-2 < x < 2$. Therefore, the W-F coupling will work when $\gamma = 10^{-3}$, corresponding to

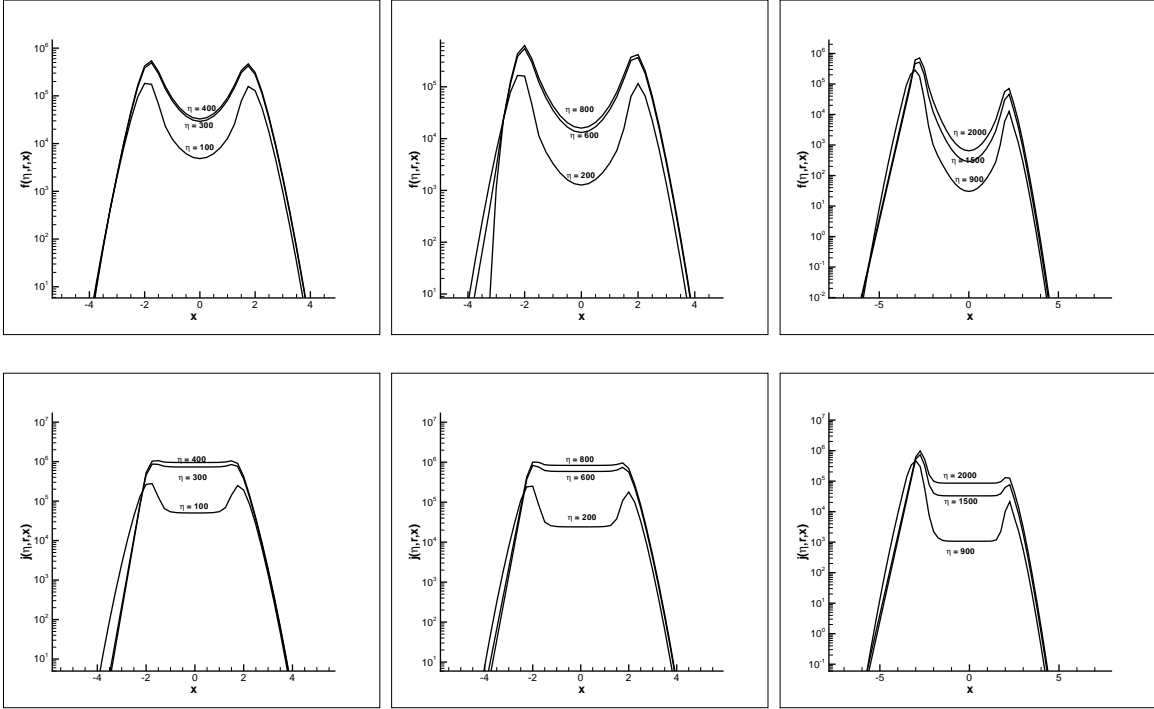


Fig. 11.— The solutions $j(\eta, r, x)$ and $f(\eta, r, x)$ of eqs.(16) and (17) at $r = 50$ (left), 100 (middle) and 500 (right). $\gamma = 10^{-3}$. The parameters are the same as those in Figures 4 and 6, except that $\gamma = 10^{-3}$.

$$f_{\text{HI}} \simeq 10^{-3}.$$

5. An example of time-dependent effect of W-F coupling on 21 cm signals

The time evolution of W-F coupling shown in §4 should be considered in calculating the 21 cm emission and absorption from the halo around the first sources. There are many self-consistent models with different parameters, such as the UV photon luminosity, frequency spectrum, the index of power law spectrum, the temperature of black-body spectrum, etc. (e.g. Cen 2006, Liu et al. 2007, Chen & Miralda-Escude 2008). But no one of these models considered the time-dependence of the W-F coupling.

To show the importance of the time-evolution of the W-F coupling, we re-calculate the brightness temperature δT_b of 21 cm signals of one of the models developed in Liu et al. (2007) where source intensity is $\dot{E} = 7.25 \times 10^{44} \text{ergs}^{-1}$ as in their Figs. 3 and 4, which is self-consistent in terms of heating and cooling of gas. The results are presented in Figure 12.

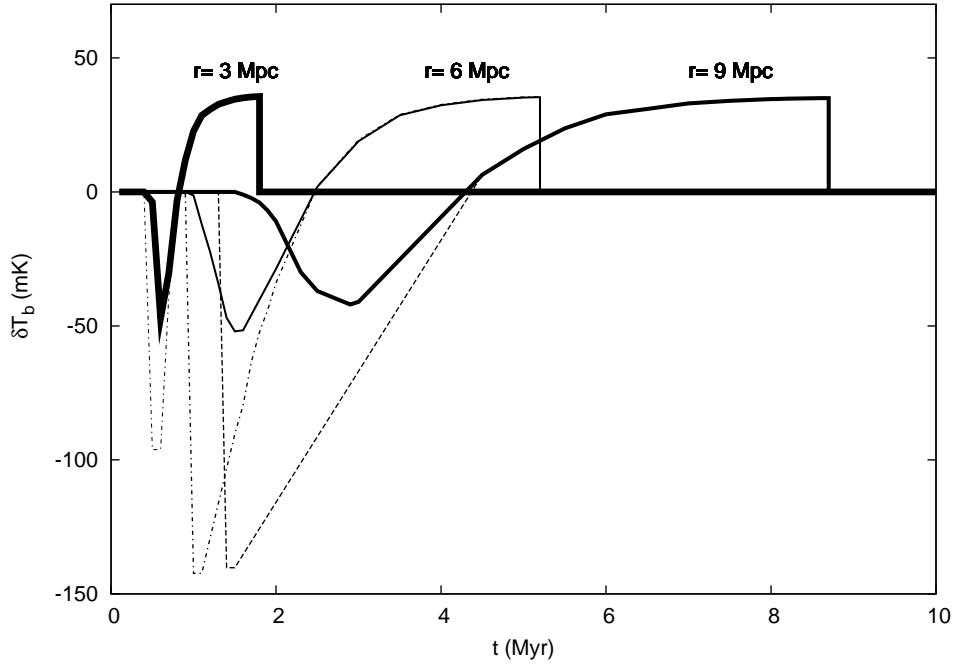


Fig. 12.— The 21 cm brightness temperature δT_b as a function of time at three comoving distances $r = 3, 6, 9$ Mpc, respectively, for the UV heating model in Liu et al (2007). The dashed lines are for the solutions with time-independent W-F coupling, while solid lines show those in which the time dependence of the W-F coupling is considered.

Figure 12 shows the time-dependence of the 21 cm brightness temperature at three shells with radius 3, 6, and 9 h^{-1} Mpc. For each radius, there are two curves, one does not consider the time-dependence of the W-F coupling, and one does. It shows that the brightness temperatures are affected by the time evolution of the W-F coupling significantly. The time dependence of the W-F coupling will make the 21 cm signals weaker, especially for absorption features by a factor 2-5. This is because absorption features are formed just after the light front passes a particular location, at a time when the intensity of Ly α photons in the Boltzmann distribution is far lower than their saturated values (Fig. 6). The absorption areas of the 21 cm signal would suffer more from insufficient Ly α photons because they are too close to the light front. On the other hand, the decrease in δT_b is negligible for emission areas.

6. Discussion and conclusions

The kinetics of Ly α resonant photons in the HI media with high optical depth τ can basically be described as diffusion in both the physical space and the frequency space. If Ly α photons do not join the diffusion in the frequency space, the transfer of Ly α photons in the physical space is very inefficient, as the number of scattering needed for escape is proportional to τ^2 . The resonant scattering of Ly α photons and neutral hydrogen makes the diffusion processes in the physical space coupled to the diffusion processes in the frequency space. First, the diffusion in the frequency space provides a shortcut for the diffusion in the physical space. It makes the mean number of scattering for escape to be approximately proportional to τ . Second, the bounce back of resonant scattering provides a mechanism of quickly restoring ν_0 photons from $x \simeq \pm(2 - 3)$ photons. Finally the W-F coupling is realized simultaneously with the restoration of the $x = 0$ photons.

The mechanism of “escape via shortcut” plus “bounce back” is mainly carried out by the photons with frequency $x \simeq \pm(2 - 3)$. In a 21 cm emission region of physical size $R \simeq 10$ kpc and $f_{\text{HI}} > 0.1$, the optical depth of $x \simeq \pm(2 - 3)$ photons is still larger than 1. Therefore, it is reasonable to use Eddington approximation. On the other hand, the optical depth of $x \simeq \pm(2 - 3)$ photons is much less than that of the $x = 0$ photons. The $x \simeq \pm(2 - 3)$ photons can transfer and enter the 21 cm emission region in a time scale less than 10^5 years. Therefore, the mechanism of “escape via shortcut” plus “bounce back” is able to timely support the W-F coupling of the 21 cm emission shell with Ly α photons from the center objects.

The time dependence of the W-F coupling would make the 21 cm signals weaker than the predication given by models which do not consider this time-evolution. Especially at the early stage of the formation of the 21 cm signal regions, the intensity of the local Boltzmann distribution is still very low, and therefore, one cannot assume that the spin temperature of 21 cm is locked to the kinetic temperature of gas. It may yield a low brightness temperature of the 21 cm signals.

Although the mechanism of “escape via shortcut” plus “bounce back” helps Ly α diffusion, it does not mean that this mechanism will reduce the Gunn-Peterson optical depth of the Ly α photons. On the contrary, the resonant scattering will lead to a slight increase of the optical depth of the Ly α in the 21 cm region, as the resonant scattering impedes the cosmic redshift (Figure 2). Consequently, there should be no observable redshifted optical signal with the frequency $\nu_0/(1 + z)$ to be spatially correlated with the $(1 + z)$ redshifted 21 cm signal.

The evolution of photons described by eqs.(16) and (17) conserves photon numbers. The

number of Ly α photons is basically conserved if one can ignore the Ly α photon destruction processes, such as the two-photon process (Spitzer & Greenstein 1951, Osterbrock, 1962). Thus, subsequent evolution of the Ly α photons in the 21 cm region is to diffuse to a large sphere around the first stars. At the same time, the Ly α photons will be redshifted. When the redshift is large enough, their Gunn-Peterson optical depth will be small, and finally these photons will escape from the halo (e.g. Miralda-Escude & Rees 1998; Loeb & Rybicki 1999; Zheng & Miralda-Escude 2002; Haiman & Cen 2005). The escaping sphere should be larger than the size of the 21 cm region. Therefore, redshifted Ly α optical signal with low surface brightness may come from a big halo around the 21 cm emission region.

This work is supported in part by the US NSF under the grants AST-0506734 and AST-0507340 and by ARO grant W911NF-08-1-0520. WX is grateful for the hospitality of National Astronomical Observatories of China, where part of this work was done.

A. Numerical algorithm

To solve equations (16) and (17) as a system, our computational domain is $(r, x) \in [0, r_{max}] \times [x_{left}, x_{right}]$, where r_{max} , x_{left} and x_{right} are chosen such that the solution vanishes to zero outside the boundaries. In the following, we describe numerical techniques involved in our algorithm, including approximations to the spatial derivatives, integrals in the frequency domain, numerical boundary condition and time evolution.

A.1. The WENO algorithm: approximations to the spatial derivatives

The spatial derivative terms in equations (16) and (17) are approximated by a fifth order finite difference WENO scheme.

We first give the WENO reconstruction procedure in approximating $\frac{\partial j}{\partial x}$,

$$\frac{\partial j(\eta^n, r_i, x_j)}{\partial x} \approx \frac{1}{\Delta x} (\hat{h}_{j+1/2} - \hat{h}_{j-1/2}), \quad (\text{A1})$$

with fixed $\eta = \eta^n$ and $r = r_i$. The numerical flux $\hat{h}_{j+1/2}$ is obtained by the fifth order WENO approximation in an upwind fashion, because the wind direction is fixed (negative). Denote

$$h_j = j(\eta^n, r_i, x_j), \quad j = -2, -1, \dots, N + 3 \quad (\text{A2})$$

with fixed n and i . The numerical flux from the WENO procedure is obtained by

$$\hat{h}_{j+1/2} = \omega_1 \hat{h}_{j+1/2}^{(1)} + \omega_2 \hat{h}_{j+1/2}^{(2)} + \omega_3 \hat{h}_{j+1/2}^{(3)}, \quad (\text{A3})$$

where $\hat{h}_{j+1/2}^{(m)}$ are the three third order fluxes on three different stencils given by

$$\begin{aligned}\hat{h}_{j+1/2}^{(1)} &= -\frac{1}{6}h_{j-1} + \frac{5}{6}h_j + \frac{1}{3}h_{j+1}, \\ \hat{h}_{j+1/2}^{(2)} &= \frac{1}{3}h_j + \frac{5}{6}h_{j+1} - \frac{1}{6}h_{j+2}, \\ \hat{h}_{j+1/2}^{(3)} &= \frac{11}{6}h_{j+1} - \frac{7}{6}h_{j+2} + \frac{1}{3}h_{j+3},\end{aligned}$$

and the nonlinear weights ω_m are given by,

$$\omega_m = \frac{\check{\omega}_m}{3}, \quad \check{\omega}_l = \frac{\gamma_l}{(\epsilon + \beta_l)^2}, \quad (\text{A4})$$

$$\sum_{l=1}^3 \check{\omega}_l$$

where ϵ is a parameter to avoid the denominator to become zero and is taken as $\epsilon = 10^{-8}$. The linear weights γ_l are given by

$$\gamma_1 = \frac{3}{10}, \quad \gamma_2 = \frac{3}{5}, \quad \gamma_3 = \frac{1}{10}, \quad (\text{A5})$$

and the smoothness indicators β_l are given by,

$$\begin{aligned}\beta_1 &= \frac{13}{12}(h_{j-1} - 2h_j + h_{j+1})^2 + \frac{1}{4}(h_{j-1} - 4h_j + 3h_{j+1})^2, \\ \beta_2 &= \frac{13}{12}(h_j - 2h_{j+1} + h_{j+2})^2 + \frac{1}{4}(h_j - h_{j+2})^2, \\ \beta_3 &= \frac{13}{12}(h_{j+1} - 2h_{j+2} + h_{j+3})^2 + \frac{1}{4}(3h_{j+1} - 4h_{j+2} + h_{j+3})^2.\end{aligned}$$

To approximate the r -derivatives in the system of equations (16) and (17), we need to perform the WENO procedure based on a characteristic decomposition. We write the left hand side of equations (16) and (17) as

$$\mathbf{u}_t + A\mathbf{u}_r \quad (\text{A6})$$

where $\mathbf{u} = (j, f)^T$ and

$$A = \begin{pmatrix} 0 & 1 \\ \frac{1}{3} & 0 \end{pmatrix}$$

is a constant matrix. To perform the characteristic decomposition, we first compute the eigenvalues, the right eigenvectors, and the left eigenvectors of A and denote them by, Λ , R and R^{-1} . We then project \mathbf{u} to the local characteristic fields \mathbf{v} with $\mathbf{v} = R^{-1}\mathbf{u}$. Now $\mathbf{u}_t + A\mathbf{u}_r$ of the original system is decoupled as two independent equations as $\mathbf{v}_t + \Lambda\mathbf{v}_r$. We approximate the derivative \mathbf{v}_r component by component, each with the correct upwind direction, with the WENO reconstruction procedure similar to the procedure described above for $\frac{\partial j}{\partial x}$. In the end, we transform \mathbf{v}_r back to the physical space by $\mathbf{u}_r = R\mathbf{v}_r$. We refer the readers to Cockburn et al. 1998 for more implementation details.

A.2. Normalization of the re-distribution term

We apply the rectangular rule to evaluate $\int R(x, x')j dx$. The rectangular rule is known to have spectral accuracy for smooth integrated function $R(x, x')j(x')$ with compact support. In equations (16) and (17), it is known that

$$\int R(x, x')dx' = \phi(x), \quad (\text{A7})$$

which is crucial for photon conservation. However,

$$\sum_j R(x, x_j)\Delta x = \phi(x)$$

may not be true in general. To numerically preserve the photon conservation, we first compute

$$ratio(x, \Delta x) = \frac{\phi(x)}{\sum_j R(x, x_j)\Delta x}, \quad (\text{A8})$$

then we normalize the collision term by approximating $\int R(x, x')j(t, r, x')dx'$ with

$$ratio(x, \Delta x) \sum_j R(x, x_j)j(\eta, r, x_j)\Delta x \quad (\text{A9})$$

with fixed η and r .

A.3. Implementation of the boundary condition

The source term given in the equation (16) is implemented as a boundary condition on $f(\eta, r = r_0, x)$.

$$f(\eta, r = r_0, x) = s_0\phi_s(x)$$

For the intensity j , a reflective boundary condition is used at $r = r_0$. At the boundary of $r = r_{max}$, $x = x_{left}$ and $x = x_{right}$, we use zero boundary conditions for both j and f , because of the way we choose r_{max} , x_{left} and x_{right} .

A.4. Time evolution

The time derivatives $\frac{\partial j}{\partial \eta}$ and $\frac{\partial f}{\partial \eta}$ are approximated by the third-order TVD Runge Kutta time discretization (Shu & Osher, 1988). For systems of ODEs $u_t = L(u)$, the third order

Runge-Kutta method is

$$\begin{aligned} u^{(1)} &= u^n + \Delta t L(u^n, t^n), \\ u^{(2)} &= \frac{3}{4}u^n + \frac{1}{4}(u^{(1)} + \Delta t L(u^{(1)}, t^n + \Delta t)), \\ u^{n+1} &= \frac{1}{3}u^n + \frac{2}{3}(u^{(2)} + \Delta t L(u^{(2)}, t^n + \frac{1}{2}\Delta t)). \end{aligned}$$

A.5. Test with the conservation of the photon number

From eq.(16) we have

$$\frac{\partial}{\partial \eta} \int j dx + \frac{\partial}{\partial r} \int f dx = 0 \quad (\text{A10})$$

Therefore, for time-independent solution we have $\int f(r, x) dx = \text{const.}$ It yields

$$\int f(r, x) dx = \int f(0, x) dx = S_0 \quad (\text{A11})$$

That is, the flux at saturated states is r -independent. This is the conservation of the number of photons. It can be used to test the algorithm.

REFERENCES

- Adams, T.F. 1972, ApJ, 174, 439
- Avery, L.W., & House, L.L. 1968, ApJ, 152, 493
- Carrillo, J.A., Gamba, I.M., Majorana, A. & Shu, C.-W. 2003, Journal of Computational Physics, 184, 498
- Carrillo, J.A., Gamba, I.M., Majorana, A. & Shu, C.-W. 2006, Journal of Computational Physics, 214, 55
- Cen, R. 2006, ApJ, 648, 47
- Chandrasekhar, S. 1943, Rev. Mod. Phys. 15, 1.
- Chen, X., & Miralda-Escude, J. 2008, ApJ, 684, 18
- Cockburn, B., Johnson, C., Shu, C-W. & Tadmor, E. 1998, Lecture Notes in Mathematics, 1697, 450

- Field, G.B., 1958, Proc. IRE, 46, 240
- Field, G.B. 1959, ApJ, 129, 551.
- Furlanetto, S.R., Oh, S.P., & Briggs, F.H. 2006, Physics Reports, 433, 181
- Haiman, Z., & Cen, R. 2005, ApJ, 623, 627
- Harrington, J.P. 1973, MNRAS, 162, 43
- Heney, L.G. 1941, Proc. Nat. Acad. Sci. 26, 50
- Hummer, D.G. 1962, MNRAS, 125, 21
- Hummer, D.G. 1965, Mem. R. astr. Soc., 70, 1
- Hummer, D.G. 1969, MNRAS, 145, 95
- Hummer, D.G. & Rybicki, G.B. 1992, ApJ, 387, 248.
- Jiang, G. & Shu, C.-W. 1996, J. Comput. Phys., 126, 202
- Liu, J.-R., Qiu, J.-M., Feng, L.-L., Shu, C.-W. & Fang, L.-Z. 2007, ApJ, 663, 1
- Loeb, A. & Rybicki, G.B. 1999, ApJ, 524, 527.
- McQuinn, M., Hernquist, L., Zaldarriaga, M. & Dutta, S. 2007, MNRAS, 381, 75
- Mihalas, D., Kunasz, P.B. & Hummer, D.G. 1976, ApJ, 210, 419
- Miralda-Escude, J. & Rees, M.J. 1998, ApJ, 497, 21
- Osterbrock, D.E. 1962, ApJ, 135, 195
- Qiu, J.-M., Feng, L.-L., Shu, C.-W. & Fang, L.-Z. 2006, New Astronomy, 12, 1
- Qiu, J.-M., Feng, L.-L., Shu, C.-W. & Fang, L.-Z. 2007, New Astronomy, 12, 398
- Qiu, J.-M., Shu, C.-W., Liu, J.-R. & Fang, L.-Z. 2008, New Astronomy, 13, 1
- Roy, I., Qiu J.-M., Shu C.-W. & Fang L.-Z., (2009b) New Astronomy 14, 513
- Roy, I. Xu, W., Qiu J.-M., Shu C.-W. & Fang L.-Z., (2009a) ApJ, 694, 1121, (PaperI)
- Rybicki, G.B. & Dell’Antonio, I.P. 1994, ApJ, 427, 603
- Shu, C.-W. & Osher, S., 1988, J. Comp. Phys., 77, 439

Spitzer, L. & Greenstein, J.L. 1951, ApJ, 114, 407

Tasitsiomi, A. 2006, ApJ, 645, 792

Wouthuysen, S. A. 1952, AJ, 57, 31

Zheng, Z. & Miralda-Escude, J., 2002, ApJ, 578, 33